AIMS Mathematics, 9(7): 18746–18762.
DOI: 10.3934/math.2024912
Received: 11 March 2024
Revised: 28 April 2024
Accepted: 06 May 2024
Published: 04 June 2024

https://www.aimspress.com/journal/Math

Research article

Machine learning approach of Casson hybrid nanofluid flow over a heated stretching surface

Gunisetty Ramasekhar[1], Shalan Alkarni[2] and Nehad Ali Shah[3,*]

[1] Department of Mathematics, Rajeev Gandhi Memorial College of Engineering and Technology (Autonomous), Nandyal 518501, Andhra Pradesh, India
[2] Department of Mathematics, College of Sciences, King Saud University, P.O. Box 2455, Riyadh 11451, Saudi Arabia
[3] Department of Mechanical Engineering, Sejong University, Seoul 05006, South Korea

*** Correspondence:** Email: nehadali199@sejong.ac.kr.

Abstract: The present investigation focused on the influence of magnetohydrodynamic Gold-Fe_3O_4 hybrid nanofluid flow over a stretching surface in the presence of a porous medium and linear thermal radiation. This article demonstrates a novel method for implementing an intelligent computational solution by using a multilayer perception (MLP) feed-forward back-propagation artificial neural network (ANN) controlled by the Levenberg-Marquard algorithm. We trained, tested, and validated the ANN model using the obtained data. In this model, we used blood as the base fluid along with Gold-Fe_3O_4 nanoparticles. By using the suitable self-similarity variables, the partial differential equations (PDEs) are transformed into ordinary differential equations (ODEs). After that, the dimensionless equations were solved by using the MATLAB solver in the Fehlberg method, such as those involving velocity, energy, skin friction coefficient, heat transfer rates and other variables. The goals of the ANN model included data selection, network construction, network training, and performance assessment using the mean square error indicator. The influence of key factors on fluid transport properties is presented via tables and graphs. The velocity profile decreased for higher values of the magnetic field parameter and we noticed an increasing tendency in the temperature profile. This type of theoretical investigation is a necessary aspect of the biomedical field and many engineering sectors.

Keywords: ANN model; Casson fluid; MHD; thermal radiation; porous medium; hybrid nanofluid
Mathematics Subject Classification: 76A05, 76R05

Nomenclature

RKF: Runge-Kutta Fehlberg method

MHD: Magnetohydrodynamic

PDE: Partial differential equation

ODE: Ordinary differential equation

x, *y*: Displacement in Cartesian coordinate system (unit: m)

u,*v*: Horizontal and vertical velocity components (unit: m/s)

U: Stretching velocity relative to stretching sheet (unit: m/s)

s_1 : First solid nanoparticle

s_2 : Second nanoparticle

f : Base fluid

nf : Nanofluid

hnf : Hybrid nanofluid

k : Thermal conductivity $(W\ m^{-1}\ K^{-1})$

ϕ_1, ϕ_2 : Nanoparticles volume fraction

σ : Electric conductivity (Sm^{-1})

β : Thermal expansion (K^{-1})

ρ : Density $(kg\ m^{-3})$

K^* : Mean absorption coefficient

T_∞ : Ambient fluid temperature, K

σ^* : Stefan Boltzmann constant

c_p : Heat capacity $(J\ kg^{-1}K^{-1})$

T_w : Surface temperature, K

T_f : Temperature of heated fluid, K

T : Temperature of the fluid, K

Pr : Prandtl number

Q : Heat absorption/generation coefficient

M : Magnetic interaction parameter

K : Porosity parameter

Rd : Radiation parameter

Fr : Inertia coefficient

α : Temperature ratio parameter

μ : Dynamic viscosity $(kg\ m^{-1}s^{-1})$

υ : Kinematic viscosity (m^2s^{-1})

$U = ax$: Stretching velocity

Subscript

': differentiation with respect to η

1. Introduction

Artificial neural networks (ANN) have played a significant role in the development of cooling equipment in the past few years. Artificial connections are frequently implemented in the heating industry for the purpose of analyzing and boiling, estimating the effectiveness of radiator mechanisms, or controlling the behaviour of heating equipment. Consequently, the investigators used the artificial

neural network (ANN) in order to do an analysis of the temperature transfer information, determine the coefficient of warmth transfer, and manage the heating element. The movement of heat from one location to another is a critical step in the process of either central heating or central cooling an item. The considerable heat that is generated must be reduced to a reasonable level or dissipated in order for a device or system to function at its highest possible standard. In order to minimize heat on equipment, such as processors, and in a number of sectors, such as automotive and technology, fluid refrigerants have historically been employed [1]. However, traditional liquid refrigerants have a weak heat transfer [2–4]. Because of this, there is a greater potential for creativity and technological improvement in the field of cooling. The use of nanofluid, which is a fluid that includes nanoparticles, is one of the methods that have been established to improve the efficiency of heat transfer in liquid refrigeration systems [3–8]. The issue with fluid containing dispersed nanometre particles is coagulation, deposition, and flow line blockage. The aforementioned issues might be partly addressed by employing nanomaterials embedded as micro particles. Nanofluids are extensively employed in semiconductors, automotive, power, and universal healthcare industries, among others, owing to their appealing high-temperature, visual, and electromagnetic characteristics [9–11].

An innovative approach of mixing two or three kinds of metallic nanoparticles within the base fluid to boost thermal performance has been developed. Hybrid nanofluid mixes metallic nanoparticles in base fluid. Using hybrid nanofluids to chill or warm machines enhances heat transmission [12–18]. Many researchers have studied nanoparticles combinations in base fluids to create a refrigerant with superior thermal conductivity. Temperature distribution and heat capacity of hybrid nanofluid are influenced by particle diameter, volume fraction, thermal efficiency, and viscosity [19–20]. Nanofluid improves material impact energy and is an excellent refrigerant. Among the several metals that are used in the study of nanofluids, alumina, due to its chemical stability and increased mechanical power, is often employed in the investigation of hybrid nanofluids. Other types of cobalt alloys are put to use in devices like jet turbines, which need high hardness. Electroplating is sometimes performed using cobalt metal because of its excellent standards, high level of hardness, and excellent corrosion resistance.

The investigation of electromagnetic flows in liquids subjected to a magnetic field is known as magnetohydrodynamics, or simply MHD. The scientific name for this phenomenon is magneto-fluid dynamics. Examples of magneto-fluids include plasmas, ions, seawater, and liquid crystals. Hanne's Alfvin was given the Nobel Prize in Physics in 1970 for his ground-breaking work in the field of MHD. The magneto-nanofluid combines the characteristics of magnets and liquids into a single substance. The magnetic impacts not only radicalize the particles in the liquid system but also create a modification in heat transfer. Additionally, the magnetic effects cause the absorption to be reconstructed. Because they contain more viscous body cells than non-malignant nanoparticles, and because the cells improve blood circulation, magnetic nanoparticles are used in the biomedical industry [21–23]. MHD has received a lot of attention in astronomy, healthcare, optical transplants, metal processing, geophysical disciplines, and petrochemical engineering [24–27].

According to the current literature, no research has been done to analyse the concept of magnetohydrodynamics (MHD) over a stretched surface with the presence of a porous medium and linear thermal radiation. The equations that are created are in the form of PDEs. To convert the PDE into ODEs, a self-similarity transformation is used. After applying transformations, for the graphical purpose, we have used the MATLAB solver in the Fehlberg scheme. In this study, we employ blood as a base fluid and Gold-Fe_3O_4 as a hybrid nanofluid. This model plays an essential role in aerospace

machinery, nuclear reactor cooling and vehicles. In the results and discussion section, graphs for different physical significance are given. As a result, the researchers are confident that the new study is unique, will have a considerable influence in the domains of engineering and mathematics, and has the opportunity to encourage new investigators.

2. Mathematical model

We consider an incompressible Casson type viscous nanofluid flow over a heated stretching surface. In addition to a stretched surface, a steady two-dimensional flow is examined in a hybrid nanofluid. The velocity components u and v are measured along the x-axis and the y-axis, respectively; $U = ax$is the stretching velocity. Furthermore, the temperature of the sheet as well as the temperature of the free stream is represented by the symbols T_f and T_∞, respectively, which are presented in Figure 1. Within the framework of the velocity equation and temperature equation, Casson fluid, porous medium, MHD, heat generation and thermal radiation are taken into account. Two distinct kinds of nanoparticles, namely Gold-Fe_3O_4 are suspended in the base fluid blood, which is demonstrated in Table 1.

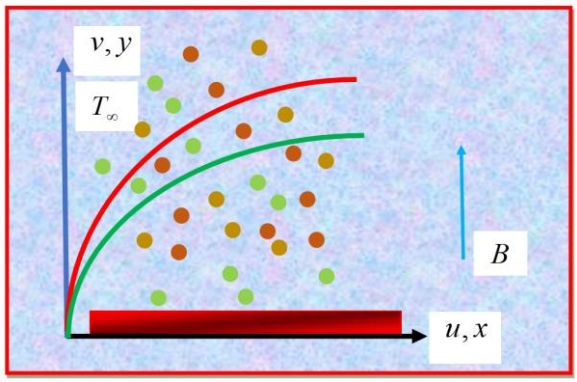

Figure 1. Flow geometry of the problem.

Table 1. Blood/Gold-Fe_3O_4 nanoparticles of thermophysical properties [34–36].

Property	Blood	Gold	Fe_3O_4
Density ρ (kgm^{-3})	1050	19,300	5200
Specific heat C_p $(Jkg^{-1}K^{-1})$	3617	129	670
Heat conductivity k_f $(Wm^{-1}K^{-1})$	0.52	318	6
Electrical conductivity σ $(\Omega m)^{-1}$	0.8	4.1×10^6	25,000
Prandtl number *(Pr)*	21		

The governing flow equations are constructed as [28–30]:

$$\frac{\partial u}{\partial x}+\frac{\partial u}{\partial y}=0, \tag{1}$$

$$u\frac{\partial u}{\partial x}+v\frac{\partial u}{\partial y}=\frac{\mu_{hnf}}{\rho_{hnf}}\left(1+\frac{1}{\Gamma}\right)\left(\frac{\partial^2 u}{\partial y^2}\right)-\frac{\mu_{hnf}}{\rho_{hnf}}\frac{u}{K^*}-\frac{\sigma_{hnf}}{\rho_{hnf}}\left(B^2u\right), \tag{2}$$

$$u\frac{\partial T}{\partial x}+v\frac{\partial T}{\partial y}=\frac{k_{hnf}}{\left(\rho c_p\right)_{hnf}}\left(\frac{\partial^2 T}{\partial y^2}\right)-\frac{1}{\left(\rho c_p\right)_{hnf}}\left(\frac{\partial q_r}{\partial y}\right)+\frac{\sigma_{hnf}B^2}{\left(\rho c_p\right)_{hnf}}u^2+\frac{Q_0}{\left(\rho c_p\right)_{hnf}}\left(T-T_\infty\right). \tag{3}$$

By the Rosseland approach, we have

$$q_r=-\frac{4\sigma^*}{3k^*}\frac{\partial T^4}{\partial y}. \tag{4}$$

By applying the Taylor's series expansion of T^4 about T_∞ and neglecting terms having higher order, we obtain

$$T^4=4T_\infty^{\ 3}T-3T_\infty^{\ 4}. \tag{5}$$

Putting Eq (5) into Eq (3), we get

$$u\frac{\partial T}{\partial x}+v\frac{\partial T}{\partial y}=\frac{k_{hnf}}{\left(\rho c_p\right)_{hnf}}\left(\frac{\partial^2 T}{\partial y^2}\right)-\frac{1}{\left(\rho c_p\right)_{hnf}}\frac{16T_\infty^3}{3k^*}\frac{\partial^2 T}{\partial y^2}+\frac{\sigma_{hnf}B^2}{\left(\rho c_p\right)_{hnf}}u^2+\frac{Q_0}{\left(\rho c_p\right)_{hnf}}\left(T-T_\infty\right). \tag{6}$$

The boundary conditions are:

$$\begin{aligned} &u=U=ax, v=0, T=T_f, \quad && at\ y=0,\\ &u\to 0, T\to T_\infty && as\ y\to\infty. \end{aligned} \tag{7}$$

The self-similarity variables are defined as:

$$u=axf'(\eta), v=-\sqrt{a\upsilon_f}\,f(\eta), \theta(\eta)=\frac{T-T_\infty}{T_f-T_\infty}, \eta=y\sqrt{\frac{a}{\upsilon_f}}. \tag{8}$$

Thermophysical properties of *hnf* are

$$A_1=\frac{\mu_{hnf}}{\mu_f}, A_2=\frac{\rho_{hnf}}{\rho_f}, A_3=\frac{(\rho c_p)_{hnf}}{(\rho c_p)_f}, A_4=\frac{k_{hnf}}{k_f}, A_5=\frac{\sigma_{hnf}}{\sigma_f}.$$

$$\left.\begin{aligned}
&\frac{\mu_{hnf}}{\mu_f}=\frac{1}{(1-\phi_1)^{2.5}(1-\phi_2)^{2.5}},\\
&\frac{\rho_{hnf}}{\rho_f}=\left\{(1-\phi_2)\left[(1-\phi_1)+\phi_1\left(\frac{\rho_{s_1}}{\rho_f}\right)\right]+\phi_2\frac{\rho_{s_2}}{\rho_f}\right\},\\
&\frac{(\rho c_p)_{hnf}}{(\rho c_p)_f}=(1-\phi_2)\left[(1-\phi_1)+\phi_1\left(\frac{(\rho c_p)_{s_1}}{(\rho c_p)_f}\right)\right]+\phi_2\frac{(\rho c_p)_{s_2}}{(\rho c_p)_f},\\
&\frac{k_{hnf}}{k_{bf}}=\frac{k_{s_1}+2k_{bf}-2\phi_2(k_{bf}-k_{s_2})}{k_{s_2}+2k_{bf}+\phi_2(k_{bf}-k_{s_2})}\times\frac{k_{s_1}+2k_f-2\phi_1(k_f-k_{s_1})}{k_{s_1}+2k_f+\phi_1(k_f-k_{s_1})},\\
&\frac{\sigma_{hnf}}{\sigma_f}=\frac{\sigma_{s_2}+2\sigma_{nf}-2\phi_2(\sigma_{nf}-\sigma_{s_2})}{\sigma_{s_2}+2\sigma_{nf}+\phi_2(\sigma_{nf}-\sigma_{s_2})}\times\frac{\sigma_{s_1}+2\sigma_f-2\phi_1(\sigma_f-\sigma_{s_1})}{\sigma_{s_1}+2\sigma_f+\phi_1(\sigma_f-\sigma_{s_1})}.
\end{aligned}\right\} \tag{9}$$

The modified dimensionless ODEs, Eqs (2) and (6) are converted by using Eq (8).

$$\frac{A_1}{A_2}f'''\left(1+\frac{1}{\Gamma}\right)+A_2\left(ff''-(f')^2\right)-\frac{A_1}{A_2}Kf'-\frac{A_5}{A_2}Mf'=0, \tag{10}$$

$$\theta''\left(A_4+\frac{4}{3}Rd\right)+A_3Prf\theta'+\frac{A_5}{A_3}MEc(f')^2+A_3PrQ\theta=0. \tag{11}$$

The boundaries of the change are described as:

$$\begin{aligned}
&f(0)=0,\ f'(0)=1,\theta'(0)=1,\\
&f'(\infty)=0,\theta'(\infty)=0.
\end{aligned} \tag{12}$$

Note that $M=\frac{\sigma_f B^2}{\rho_f a}$ is the magnetic field parameter, $Pr=\frac{\mu_f\left(c_p\right)_f}{k_f}$ is the Prandtl number, $Rd=\frac{4\sigma^* T_\infty^3}{k^* k_f}$ is the radiation parameter, $Ec=\frac{U^2}{c_p\left(T_f-T_\infty\right)}$ is the Eckert number, $K=\frac{\upsilon_f}{aK^*}$ is the porosity parameter, and $Q=\frac{Q_0}{a\left(\rho C_p\right)_f}$ is the heat absorption/generation.

The dimensional form of C_f, and *Nu* are defined as

$$C_f=\frac{\tau_w}{\rho_f U^2}, \tag{13}$$

where shear stress τ_w is

$$\tau_w = \mu_{hnf} \left. \frac{\partial u}{\partial y} \right|_{y=0}.$$

$$Nu = \frac{x q_w}{k_f \left(T_w - T_\infty \right)}, \tag{14}$$

where heat flux q_w is

$$q_w = -k_{hnf} \left. \frac{\partial T}{\partial y} \right|_{y=0}.$$

The non-dimensional form of Eqs (13) and (14) are:

$$Re_r^{1/2} C_f = A_1 f''(0), \tag{15}$$

$$Re_r^{-1/2} Nu_r = -A_4 \theta'(0). \tag{16}$$

Where Re_r is the local Reynolds number.

3. Numerical scheme

In order to solve the nonlinear ODE system consisting of Eqs (10) and (11) and the boundary conditions, Eqs (12) all that is required is to enter data into the Fehlberg method function that is included inside MATLAB. At the beginning of the procedure, Eqs (10)–(12) are transformed into a collection of related first-order equations. This is done in order to make it possible for the Fehlberg technique to be used in the MATLAB (R2020b) solver. The numerical findings are shown for a variety of values of the factors that have been taken into consideration in this particular research endeavor. In the present model, we used the step size $\Delta\eta = 0.01$ and which is the standard used for convergence. When performing the inner iteration, criteria for convergence are consistently employed. In the present investigation, a relative tolerance of error 10^{-8} is taken into account.

4. Design of artificial neural network modelling

An artificial neural network (ANN) is a type of concurrently processed design made up of various levels of relatively straightforward producers named neurons that are all highly linked to each other. An ANN is a computational framework and high-tech computer instrument which employs neuro-computing for handling data. The ANN is capable of both matching patterns and neural network learning. The human nervous system served as the inspiration for the development of the aforementioned model, which has computational features that are identical to those of the actual physical cell. Our brain has the capacity to perform enormous computations and makes use of the trillions of sensory neurons that are present in the skull. In contrast with neurons in real life, artificial neural networks retain input as weighted interconnections, rather than storing it in storage. When

employing this method, the establishment of structural characteristics may be accomplished more quickly and with a reduced number of calculations. Both input and output levels, in addition to a secret layer that comprises components that turn information into output so that the layer that generates results may utilize the outcome to make decisions, constitute the components that make up artificial neural networks (ANNs). Artificial brains have the ability to extract significant information from erroneous data as they are used to identify patterns and generate characteristics which are difficult for both computers and people to characterize. The design of the ANN is presented in Figure 2(a). The ANN algorithm was tested, proven, and trained using different sets of data. Seventy percent of the information provided was employed for training, fifteen percent for validation, and fifteen percent for testing the findings of the present model. Figure 2(b) demonstrates a back propagation of the neural network. Figure 3 illustrates the outcomes of the $C_f Re_r^{1/2}$ measurements that were performed on the ANN model in the ANN performance, initial training and Regression lines for skin friction. Figure 4 shows that the outcomes of the $Nu_r Re_r^{-1/2}$ measurements that were performed on the ANN model in the ANN performance, initial training and Regression lines for Nusselt number. All of the necessary parameters are provided to the machine learning models so that they may represent the intricate relationship among the two sets of data. The ANN algorithm's outputs are quite consistent with the computed numbers [31–33].

At the moment, the ANN model MLP that is both the most popular and exciting is the feed-forward neural network (FFNN). This model is based on a perception architecture that has numerous layers. During the process of determining the error in the network's output, the method known as back propagation may be used to rearrange the relative weights of each of the cells. Back propagation delivers the greatest outcomes when it comes to training FFNNs. This is the case by a considerable margin and by a significant amount of success. In general, it may assist in reducing the amount of mistakes that occur.

The j^{th} hidden neuron receives the following as its net input:

$$y_j(x) = \sum_{i=1}^{1} W1_{ji} x_i + a_j.$$

In this notation, x_i represents the input layer of the i^{th} node, a_j represents the hidden layer of the j^{th} node, and $W1_{ji}$ stands for the linking weight between x_i and a_j.

Here is a representation of the j^{th} hidden node in the output:

$$z_j(x) = \frac{1}{1+e^{-y_j(x)}}.$$

The next equation pertains to the layer's k^{th} output node:

$$o_k(x) = \sum_{j=1}^{m} W2_{kj} z_j + b_k.$$

If node k in the output layer is connected to node j in the hidden layer, then the weight $W2_{kj}$ indicates the strength of that relationship. In addition, the word "bias" is denoted by the variable "b_k" and is located at the k^{th} node of the output layer.

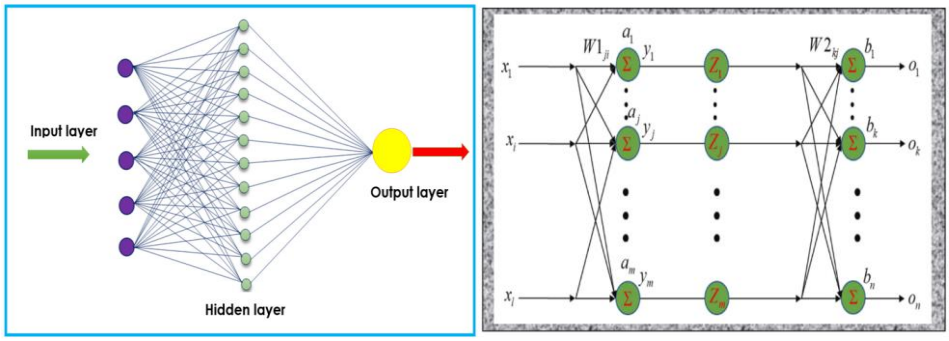

(a) (b)

Figure 2. (a) The design of the ANN; **(b)** Back propagation of the neural network.

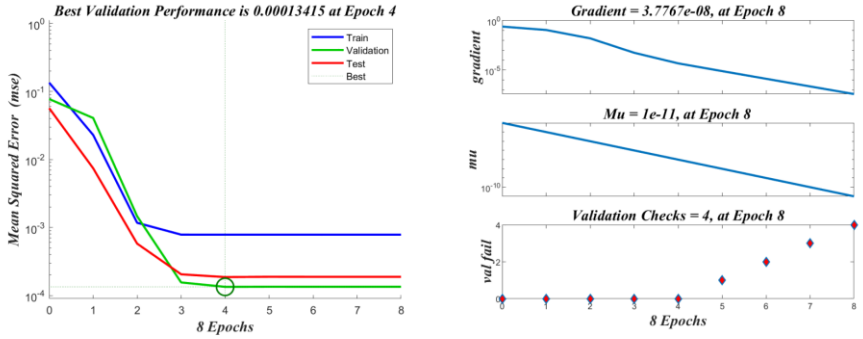

(a) (b)

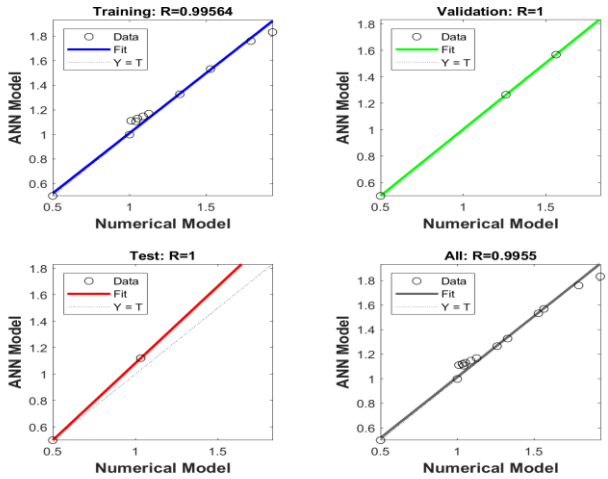

(c)

Figure 3. (a) ANN performance; **(b)** ANN training; **(c)** Regression lines for $C_f Re_r^{1/2}$.

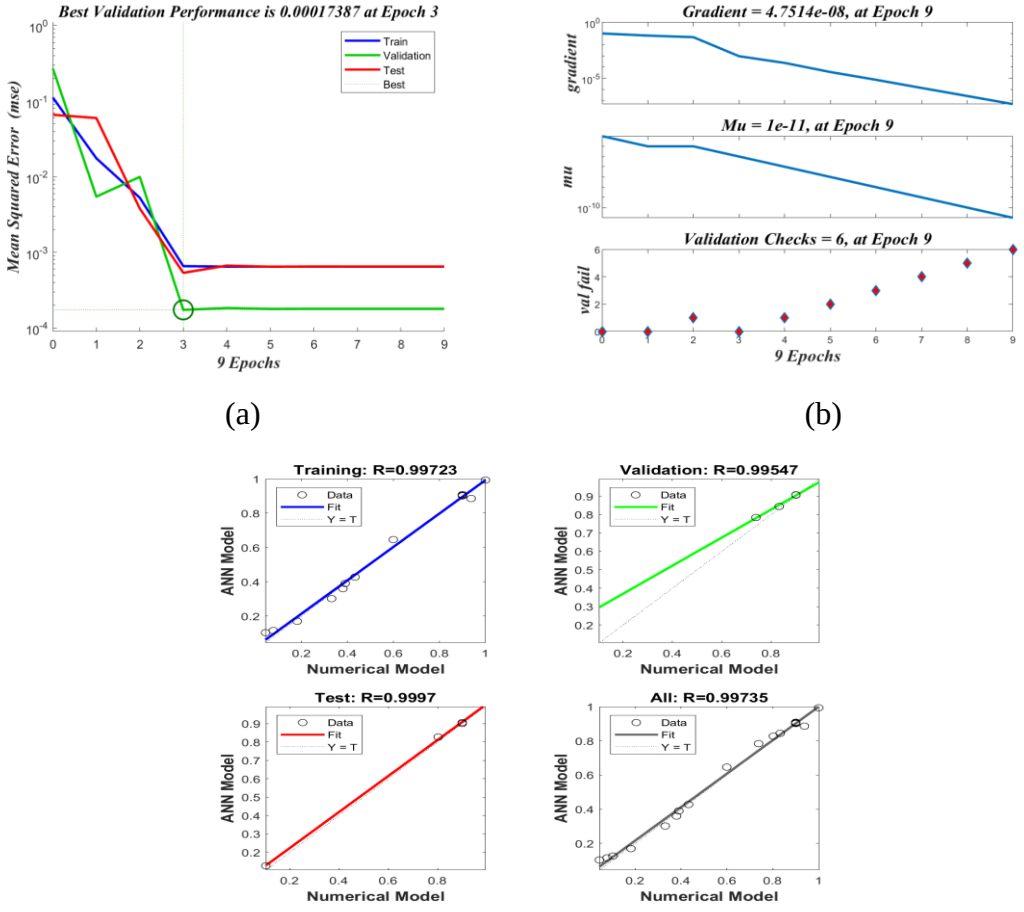

Figure 4. (a) ANN performance; **(b)** ANN training; **(c)** Regression lines for $Nu_r Re_r^{-1/2}$.

5. Results and discussion

The non-dimensional Eqs (10) and (11), along with the boundary Eq (12), might be answered numerically using the help provided by the MATLAB solver according to the Fehlberg method. The numerical values of the non-dimensional variables were taken and used for evaluation. The precise results are shown in Tables 2–4, which demonstrate the variations in the skin friction coefficient along with ANN outputs. The findings of both investigations were determined to be fairly accurate.

Table 2. Comparison table for various *Pr* of the current study.

Pr	Ali et al. [28]	Present results
0.7	0.4560	0.455322
2.0	0.9113	0.910337

Table 3. Values of the $C_f Re_r^{1/2}$ for various parameters.

M	***K***	***Ec***	**Numerical model** $C_f Re_r^{1/2}$	**ANN model**
0.1	0.3	0.5	1.528030	1.52803002
0.1	0.3	0.5	1.259748	1.25974804
0.1	0.3	0.5	1.791082	1.79108292
0.1	0.3	0.5	1.125601	1.12560183
0.1	0.3	0.5	1.033058	1.03305894
1.0	1.0	1.0	1.041283	1.04128301
0.1	0.3	0.5	1.053002	1.05300224
0.1	0.3	0.5	1.010293	1.01029305
0.1	0.3	0.5	1.088258	1.08825804
0.1	0.3	0.5	1.564001	1.56400162
0.1	0.3	0.5	1.033502	1.03350294
0.1	0.3	0.5	1.932038	1.93203882

Table 4. Values of $Nu_r Re_r^{-1/2}$ for various parameters.

Pr	***M***	***Rd***	***Q***	**Numerical model** $Nu_r Re_r^{-1/2}$	**ANN model**
0.62	0.5	0.7	0.9	0.0436	0.043602
0.62	0.5	0.7	0.9	0.0772	0.077273
0.62	0.5	0.7	0.9	0.3800	0.380065
0.62	0.5	0.7	0.9	0.1024	0.102449
0.62	0.5	0.7	0.9	0.8025	0.802538
1.0	1.0	1.0	1.0	0.3900	0.390002
0.62	0.5	0.7	0.9	0.5993	0.599330
0.62	0.5	0.7	0.9	0.1811	0.181125
0.62	0.5	0.7	0.9	0.4326	0.432602
0.62	0.5	0.7	0.9	0.7381	0.738116
0.62	0.5	0.7	0.9	0.8324	0.832436
0.62	0.5	0.7	0.9	0.9380	0.938016

The influence of *M* on the velocity sketch is seen in Figure 5(a). It can be seen that the velocity profile has a decreasing trend for higher *M* values, which indicates that the value of *M* is increasing. Physically speaking, an increase in *M* causes a Lorentz force to be produced, which retards the movement of the liquid. As a consequence of the fact that the Lorentz force is antagonistic to the motion of fluids, the flow velocity decreases as a consequence of the increased resistance, which in turn leads to a declined in the velocity profile. When increases in the *K* values improves the velocity outline, which is demonstrated in Figure 5(b), physically by raising the *K* values, a porous substance becomes more difficult to flow across, retarding the flow of fluids. As a direct and immediate consequence of this, the dimension of the outermost boundary layer is decreased.

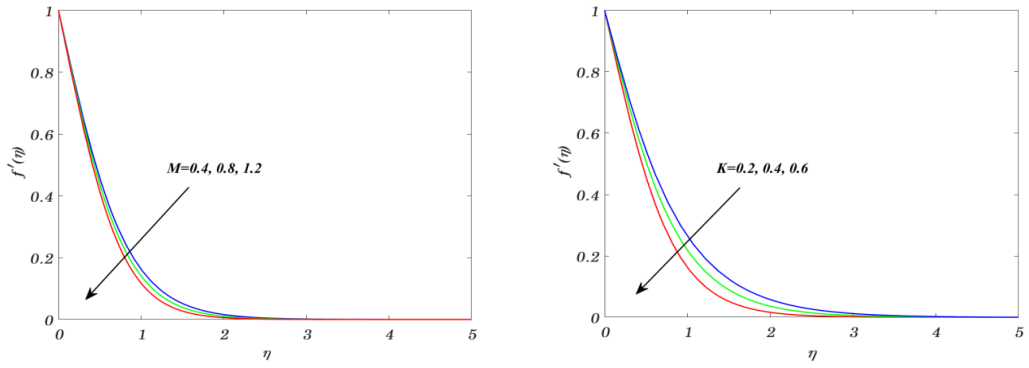

(a) (b)

Figure 5. (a) Pictogram of M on $f'(\eta)$; **(b)** Pictogram of on K $f'(\eta)$.

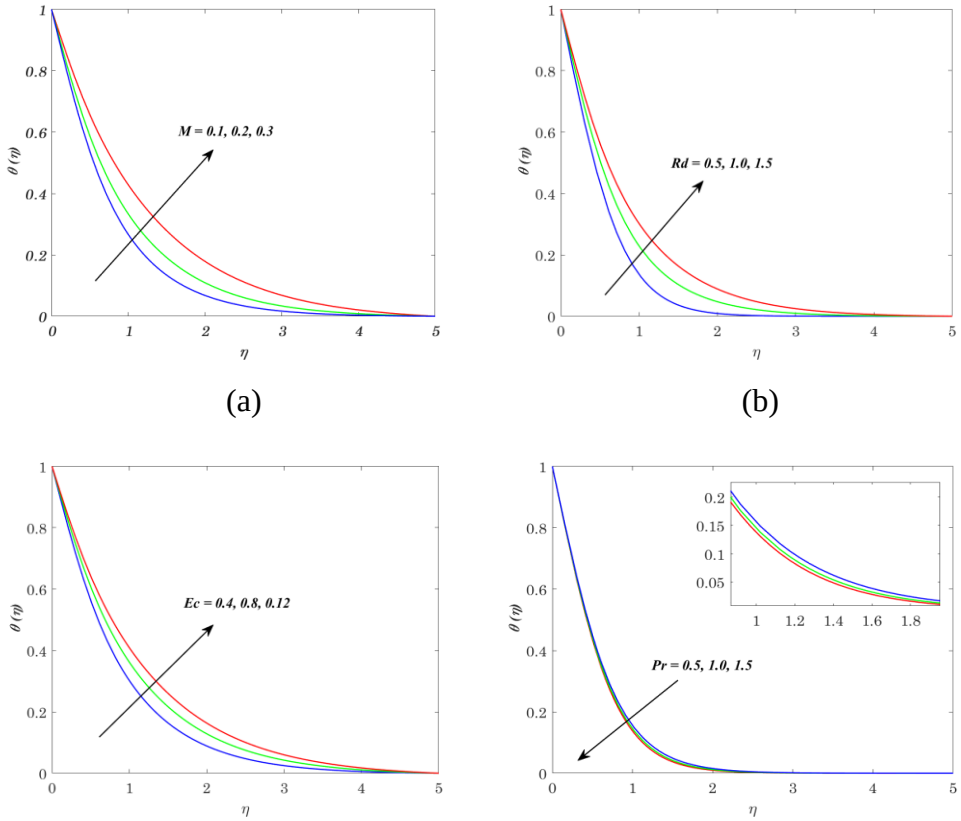

(a) (b)

(c) (d)

Figure 6. (a) Pictogram of M on $\theta(\eta)$; **(b)** Pictogram of Rd on $\theta(\eta)$; **(c)** Pictogram of Ec on $\theta(\eta)$; **(d)** Pictogram of Pr on $\theta(\eta)$.

The effect of the magnetic field on the temperature profile is seen in Figure 6(a). It states that growing the M parameter increased the energy outline. This enhancement is due to the fact that the

addition of *M* into an electrically conducting material produces a resistive Lorentz force. This kind of force has the ability to raise the fluid's temperature. So, this is the reason that the temperature profile enhances. Figure 6(b) shows the radiation parameter temperature profile features. Physically, thermal radiation is the radiant energy released by all generators above zero. Electromagnetic radiation from heated surfaces rotates atoms in matter, generating kinetic energy. The graph demonstrates how increasing radiation enhances heat transmission. When *Rd* is raised, more heat is transmitted into the liquid, strengthening the thermal barrier. Since the mean absorption coefficient drops as radiation growths, temperature also increases. The effect of the Eckert number on the energy profile is seen in Figure 6(c). It states that growing the *Ec* values enhances the energy outline. Physically, *Ec* generates the frictional force that causes the fluid temperature increased. The influence of *Pr* on the energy profile is seen in Figure 6(d). It states that increasing the *Pr* values enhanced the temperature profile. The thermal dissipation of the liquid essentially reduces, resulting in a declined in the energy profile.

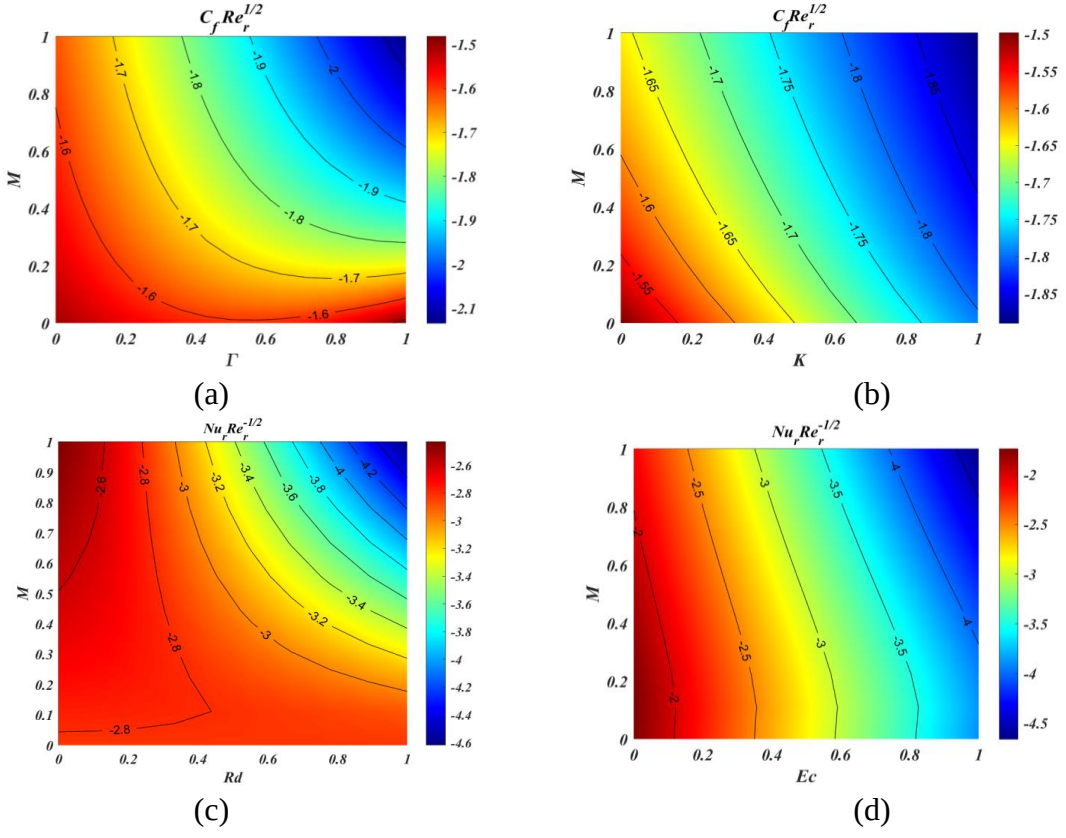

Figure 7. (a) Sway of M *and* Γ on $C_f Re_r^{1/2}$; **(b)** Sway of M *and* K on $C_f Re_r^{1/2}$; **(c)** Sway of M *and* Rd on $Nu_r Re_r^{-1/2}$; **(d)** Sway of M *and* Ec on $Nu_r Re_r^{-1/2}$.

Figures 7(a) and (b) display the influence of Γ, K, and M on the $C_f Re_r^{1/2}$. It shows that the skin friction factor is decreasing for the greater values of *K*, while we observed the reverse nature in Figure 7(b). Figures 7(c) and (d) demonstrate the inspiration of the *Ec*, *Rd* and magnetic field on the $Nu_r Re_r^{-1/2}$ profile. It shows that the *Nu* enhanced in all cases with greater values of *Rd* and the magnetic field. Streamlines, when applied to the study of fluid dynamics and the representation of flow, have a number of advantages that, considered together, allow them to be efficient tools for comprehending and studying fluid movement. Figures 8(a) and (b) exhibit magnetic parameters for various values of

M= 0.2, 0.4 influences on streamline plots. Magnetic parameter strength draws electrical conductivity molecules more toward the main stream.

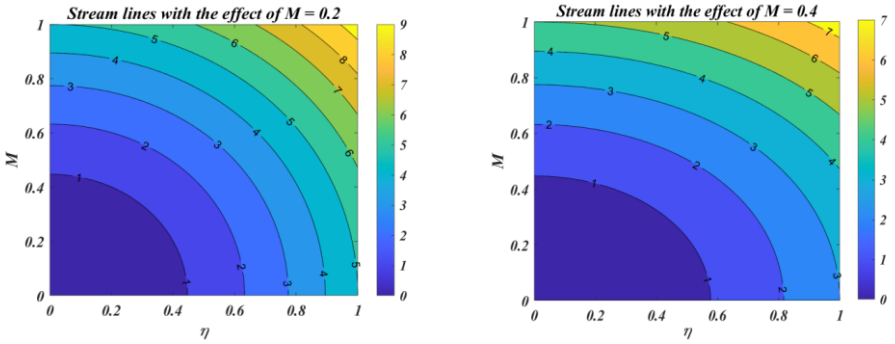

(a) (b)

Figure 8. (a) Stream lines for $M = 0.2$; **(b)** Stream lines for $M = 0.4$.

6. Conclusions

An investigation of a numerical model used in the MHD of a hybrid nanofluid composed of Gold-Fe_3O_4 and blood was carried out in the present investigation. The mathematical system's PDEs are converted into matching ODEs that show the issue's dynamics and the results are numerically solved by using the Fehlberg technique. The findings were displayed in a various visual style, such as streamlines, surface plots in three dimensions and 2-dimensional figures. The research produced a number of interesting findings, which are listed below:

- Obtaining accurate forecasts for reality via the integration of neural networks and artificial intelligence.
- Velocity profile decreases for the greater values of the magnetic field and porosity parameter values.
- The temperature profile improved with an improvement in the radiation parameter.
- The skin friction factor slowly increased for the larger values of the porous parameter.
- The *Nu* profile enhanced, for the increasing values of *M* and *Rd*.
- Streamlines are oscillating character, which is necessary for magnifying the magnetic field parameter.

Author contributions

Conceptualization, GR and NAS; Data curation, GR and SA, Formal Analysis, SA; Investigation, NAS; Methodology, SA and NAS; Software, SA; Validation, NAS; Writing–original draft, GR; Writing–review & editing, SA and NAS.

Use of AI tools declaration

The authors declare they have not used Artificial Intelligence (AI) tools in the creation of this article.

Acknowledgments

This project was supported by Researchers Supporting Project number (RSPD2024R909), King Saud University, Riyadh, Saudi Arabia.

Conflict of interest

All authors declare no conflicts of interest in this paper.

References

1 M. Sheikholeslami, *Application of control volume based finite element method (CVFEM) for nanofluid flow and heat transfer*, Elsevier, 2019. https://doi.org/10.1016/C2017-0-01264-8

2 S. K. Das, S. U. S. Choi, H. E. Patel, Heat transfer in nanofluids—A review, *Heat Transfer Eng.*, **27** (2006), 3–19. https://doi.org/10.1080/01457630600904593

3 G. Ramasekhar, P. B. A. Reddy, Entropy generation on Darcy–Forchheimer flow of Copper-Aluminium oxide/Water hybrid nanofluid over a rotating disk: Semi-analytical and numerical approaches, *Sci. Iran.*, **30** (2023), 2245–2259. https://doi.org/10.24200/sci.2023.60134.6617

4 S. R. R. Reddy, G. Ramasekhar, S. Suneetha, S. Jakeer, Entropy generation analysis on MHD $Ag^{+}Cu$/blood tangent hyperbolic hybrid nanofluid flow over a porous plate, *J. Comput. Biophys. Chem.*, **22** (2023), 881–895. https://doi.org/10.1142/S2737416523500473

5 B. A. Bhanvase, D. P. Barai, S. H. Sonawane, N. Kumar, S. S. Sonawane, Intensified heat transfer rate with the use of nanofluids, In: *Handbook of nanomaterials for industrial applications*, Elsevier, 2018, 739–750. https://doi.org/10.1016/B978-0-12-813351-4.00042-0

6 S. R. R. Reddy, P. B. A. Reddy, A. M. Rashad, Activation energy impact on chemically reacting eyring–powell nanofluid flow over a stretching cylinder, *Arab. J. Sci. Eng.*, **45** (2020), 5227–5242. https://doi.org/10.1007/s13369-020-04379-9

7 H. Tahir, U. Khan, A. Din, Y. M. Chu, N. Muhammad, Heat transfer in a ferromagnetic chemically reactive species, *J. Thermophys. Heat Transf.*, **35** (2021), 402–410.

8 N. S. Khashi'ie, N. M. Arifin, I. Pop, N. S. Wahid, Flow and heat transfer of hybrid nanofluid over a permeable shrinking cylinder with Joule heating: A comparative analysis, *Alex. Eng. J.*, **59** (2020), 1787–1798. https://doi.org/10.1016/j.aej.2020.04.048

9 M. Gupta, V. Singh, R. Kumar, Z. Said, A review on thermophysical properties of nanofluids and heat transfer applications, *Renew. Sust. Energ. Rev.*, **74** (2017), 638–670. https://doi.org/10.1016/j.rser.2017.02.073

10 B. Mehta, D. Subhedar, H. Panchal, Z. Said, Synthesis, stability, thermophysical properties and heat transfer applications of nanofluid—A review, *J. Mol. Liq.*, **364** (2022), 120034. https://doi.org/10.1016/j.molliq.2022.120034

11 S. U. S. Choi, J. A. Eastman, *Enhancing thermal conductivity of fluid with nanoparticles*, 1995.

12 S. Jakeer, P. B. A. Reddy, Entropy generation on the variable magnetic field and magnetohydrodynamic stagnation point flow of Eyring–Powell hybrid dusty nanofluid: Solar thermal application, *P. I. Mech. Eng. C-J. Mec.*, **236** (2022), 7442–7455. https://doi.org/10.1177/09544062211072457

13 N. S. M. Hanafi, W. A. W. Ghopa, R. Zulkifli, S. Abdullah, Z. Harun, M. R. A. Mansor, Numerical simulation on the effectiveness of hybrid nanofluid in jet impingement cooling application, *Energy Rep.*, **8** (2022), 764–775. https://doi.org/10.1016/j.egyr.2022.07.096

14 M. M. Bhatti, R. Ellahi, Numerical investigation of non-Darcian nanofluid flow across a stretchy elastic medium with velocity and thermal slips, *Numer. Heat Tr. B- Fund.*, **83** (2023), 323–343. https://doi.org/10.1080/10407790.2023.2174624

15 M. M. Bhatti, O. A. Bég, S. Kuharat, Electromagnetohydrodynamic (EMHD) convective transport of a reactive dissipative carreau fluid with thermal ignition in a non-Darcian vertical duct, *Numer. Heat Tr. A-Appl.*, 2023, 1–31. https://doi.org/10.1080/10407782.2023.2284333

16 R. Raza, R. Naz, S. Murtaza, S. I. Abdelsalam, Novel nanostructural features of heat and mass transfer of radiative Carreau nanoliquid above an extendable rotating disk, *Int. J. Mod. Phys. B*, 2024. https://doi.org/10.1142/S0217979224504071

17 S. I. Abdelsalam, W. Abbas, A. M. Megahed, A. A. M. Said, A comparative study on the rheological properties of upper convected Maxwell fluid along a permeable stretched sheet, *Heliyon*, **9** (2023), e22740.https://doi.org/10.1016/j.heliyon.2023.e22740

18 M. M. Bhatti, K. Vafai, S. I. Abdelsalam, The role of nanofluids in renewable energy engineering, *Nanomaterials*, **13** (2023), 2671. https://doi.org/10.3390/nano13192671

19 W. H. Azmi, S. N. M. Zainon,K. A. Hamid, R. Mamat, A review on thermo-physical properties and heat transfer applications of single and hybrid metal oxide nanofluids, *J. Mech. Eng. Sci.*, **13** (2019), 5182–5211. https://doi.org/10.15282/jmes.13.2.2019.28.0425

20 G. Ramasekhar, Scrutinization of BVP Midrich method for heat transfer analysis on various geometries in the presence of porous medium and thermal radiation, *J. Nanofluids*, **13** (2024), 100–107. https://doi.org/10.1166/jon.2024.2130

21 S. Arulmozhi, K. Sukkiramathi, S. S. Santra, R. Edwan, U. Fernandez-Gamiz, S. Noeiaghdam, Heat and mass transfer analysis of radiative and chemical reactive effects on MHD nanofluid over an infinite moving vertical plate, *Results Eng.*, **14** (2022), 100394. https://doi.org/10.1016/j.rineng.2022.100394

22 S. R. R. Reddy, P. B. A. Reddy, Thermal radiation effect on unsteady three-dimensional MHD flow of micropolar fluid over a horizontal surface of a parabola of revolution, *Propuls. Power Res.*, **11** (2022), 129–142. https://doi.org/10.1016/j.jppr.2022.01.001

23 S. Jakeer, B. A. R. Polu, Homotopy perturbation method solution of magneto-polymer nanofluid containing gyrotactic microorganisms over the permeable sheet with Cattaneo–Christov heat and mass flux model, *P. I. Mech. Eng. E-J. Pro.*, **236** (2022), 525–534. https://doi.org/10.1177/09544089211048993

24 S. Jakeer, P. B. A. Reddy, Entropy generation on EMHD stagnation point flow of hybrid nanofluid over a stretching sheet: Homotopy perturbation solution, *Phys. Scr.*, **95** (2020), 125203. https://doi.org/10.1088/1402-4896/abc03c

25 H. Ge-Jile, N. A. Shah, Y. M. Mahrous, P. Sharma, C. S. K. Raju, S. M. Upddhya, Radiated magnetic flow in a suspension of ferrous nanoparticles over a cone with brownian motion and thermophoresis, *Case Stud. Therm. Eng.*, **25** (2021), 100915. https://doi.org/10.1016/j.csite.2021.100915

26 M. Yaseen, S. K. Rawat, N. A. Shah, M. Kumar, S. M. Eldin, Ternary hybrid nanofluid flow containing gyrotactic microorganisms over three different geometries with Cattaneo–Christov model, *Mathematics*, **11** (2023), 1237. https://doi.org/10.3390/math11051237

27 P. Ragupathi, N. A. Ahammad, A. Wakif, N. A. Shah, Y. Jeon, Exploration of multiple transfer phenomena within viscous fluid flows over a curved stretching sheet in the co-existence of gyrotactic micro-organisms and tiny particles, *Mathematics*, **10** (2022), 4133. https://doi.org/10.3390/math10214133

28 M. Ramzan, F. Ali, N. Akkurt, A. Saeed, P. Kumam, A. M. Galal, Computational assesment of Carreau ternary hybrid nanofluid influenced by MHD flow for entropy generation, *J. Magn. Magn. Mater.*, **567** (2023), 170353. https://doi.org/10.1016/j.jmmm.2023.170353

29 G. Ramasekhar, P. B. A. Reddy, Entropy generation on EMHD Darcy-Forchheimer flow of Carreau hybrid nano fluid over a permeable rotating disk with radiation and heat generation : Homotopy perturbation solution, *P. I. Mech. Eng. E-J. Pro.*, **237** (2023), 1179–1191. https://doi.org/10.1177/09544089221116575

30 G. Rasool, A. J. Chamkha, T. Muhammad, A. Shafiq, I. Khan, Darcy-forchheimer relation in Casson type MHD nanofluid flow over non-linear stretching surface, *Propuls. Power Res.*, **9** (2020), 159–168. https://doi.org/10.1016/j.jppr.2020.04.003

31 P. B. A. Reddy, R. Das, Estimation of MHD boundary layer slip flow over a permeable stretching cylinder in the presence of chemical reaction through numerical and artificial neural network modeling, *Eng. Sci. Technol.*, **19** (2016), 1108–1116. https://doi.org/10.1016/j.jestch.2015.12.013

32 S. Tian, N. I. Arshad, D. Toghraie, S. A. Eftekhari, M. Hekmatifar, Using perceptron feed-forward Artificial Neural Network (ANN) for predicting the thermal conductivity of graphene oxide-Al_2O_3/water-ethylene glycol hybrid nanofluid, *Case Stud. Therm. Eng.*, **26** (2021), 101055. https://doi.org/10.1016/j.csite.2021.101055

33 S. Jakeer, M. L. Rupa, S. R. R. Reddy, A. M. Rashad, Artificial neural network model of non-Darcy MHD Sutterby hybrid nanofluid flow over a curved permeable surface: Solar energy applications, *Propuls. Power Res.*, **12** (2023), 410–427. https://doi.org/10.1016/j.jppr.2023.07.002

34 C. G. N. Ketchate, P. T. Kapen, D. Fokwa, G. Tchuen, Stability analysis of non-Newtonian blood flow conveying hybrid magnetic nanoparticles as target drug delivery in presence of inclined magnetic field and thermal radiation: Application to therapy of cancer, *Inform. Med. Unlocked*, **27** (2021), 100800. https://doi.org/10.1016/j.imu.2021.100800

35 U. Khan, A. Zaib, A. Ishak, Magnetic field effect on Sisko fluid flow containing gold nanoparticles through a porous curved surface in the presence of radiation and partial slip, *Mathematics*, **9** (2021), 921. https://doi.org/10.3390/math9090921

36 M. A. Basit, U. Farooq, M. Imran, N. Fatima, A. Alhushaybari, S. Noreen, et al., Comprehensive investigations of (Au-Ag/Blood and Cu-Fe_3O_4/Blood) hybrid nanofluid over two rotating disks: Numerical and computational approach, *Alex. Eng. J.*, **72** (2023), 19–36. https://doi.org/10.1016/j.aej.2023.03.077